

Van der Waals magnetic-electrode transfer for two-dimensional spintronic devices

Zhongzhong Luo^{1,3}, Zhihao Yu^{3,4}, Xiangqian Lu⁵, Wei Niu⁶, Yao Yu⁴, Yu Yao⁷, Fuguo Tian⁷, Chee Leong Tan⁴, Huabin Sun^{3,4}, Li Gao^{6,7}, Wei Qin^{5}, Yong Xu^{3,4*}, Qiang Zhao^{1,7*} and Xiang-Xiang Song^{2,8*}*

¹College of Electronic and Optical Engineering & College of Flexible Electronics (Future Technology), State Key Laboratory of Organic Electronics and Information Displays, Nanjing University of Posts and Telecommunications, Nanjing 210023, China

²CAS Key Laboratory of Quantum Information, University of Science and Technology of China, Hefei, 230026, China

³Guangdong Greater Bay Area Institute of Integrated Circuit and System, Guangzhou 510535, China

⁴College of Integrated Circuit Science and Engineering, Nanjing University of Posts and Telecommunications, Nanjing 210023, China

⁵School of Physics, State Key Laboratory of Crystal Materials, Shandong University, Jinan 250100, China

⁶School of Science, Nanjing University of Posts and Telecommunications, Nanjing 210023, China

⁷Institute of Advanced Materials, Nanjing University of Posts and Telecommunications, Nanjing 210023, China

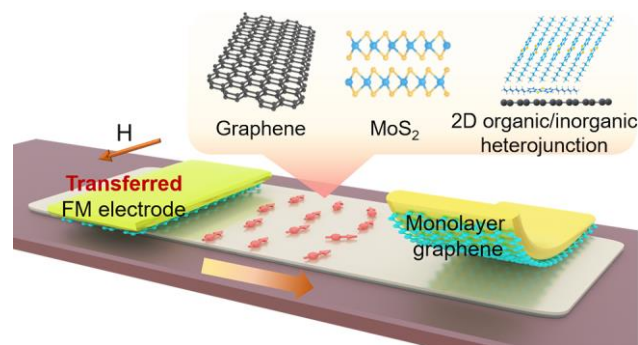
⁸Suzhou Institute for Advanced Research, University of Science and Technology of China Suzhou, 215123, China

* Correspondence should be addressed to X.-X.S. (songxx90@ustc.edu.cn), Q.Z. (iamqzhao@njupt.edu.cn), Y.X. (xuyong@njupt.edu.cn) or W.Q. (wqin@sdu.edu.cn)

ABSTRACT

Two-dimensional (2D) materials are promising candidates for spintronic applications. Maintaining their atomically-smooth interfaces during integrating ferromagnetic (FM) electrodes is crucial since conventional metal deposition tends to induce defects at the interfaces. Meanwhile, the difficulties in picking up FM metals with strong adhesion, and in achieving conductance match between FM electrodes and spin transport channels make it challenging to fabricate high-quality 2D spintronic devices using metal transfer techniques. Here, we report a solvent-free magnetic-electrode transfer technique that employs a graphene layer to assist in transferring FM metals. It also serves as part of the FM electrode after transfer for optimizing spin injection, enabling realization of spin valves with excellent performance based on various 2D materials. In addition to two-terminal devices, we demonstrate that the technique is applicable for four-terminal spin valves with non-local geometry. Our results provide a promising future of realizing 2D spintronic applications using the developed magnetic-electrode transfer technique.

TOC



KEYWORDS

magnetic-electrode transfer technique, spin valves, solvent-free, two-dimensional materials, high-quality interfaces, spintronics

Since the discovery of graphene, a variety of two-dimensional (2D) materials have attracted significant research interests for spintronic applications.¹⁻⁸ For example, graphene is recognized as a promising material for spin channel due to its long spin diffusion length l_{sf} and high carrier mobility up to room temperature.⁹⁻¹¹ The intrinsic spin-orbit coupling and the bandgap in semiconducting transition metal dichalcogenides provide powerful knobs for electrically controlling the device magnetoresistance (MR) and manipulating spins they host.¹²⁻¹⁵ Besides, owing to the weak spin-orbit coupling and hyperfine interaction,¹⁶⁻¹⁸ 2D organic materials are expected to carry spins with long life time, which are essential for spintronic applications.

To unlock the great potentials that 2D materials host for spintronic devices, it is highly desirable to maintain high-quality interfaces during integrating ferromagnetic (FM) metals for spin injection.¹⁹⁻²¹ This is technically challenging because of two reasons. One is conventional fabrication processes, such as electron beam lithography and metal deposition, tend to create defects, strain, disorder and metal diffusion at metal/2D material interfaces.²² The other is the difficulties in achieving good conductance match between FM electrodes and spin transport channels.²³ Recently, van der Waals (vdW) metal transfer techniques have been developed and are demonstrated to be powerful for realizing atomically-smooth non-magnetic metal/2D semiconductor interfaces.^{22, 24-27} However, their capability in spintronic applications^{28, 29} remains highly unexplored, since 1) FM metals are usually difficult to be picked up due to their strong adhesion to substrates; 2) the obtained tunnel barriers at the contacts are usually too transparent for spin injection which need to be adjusted.

Here, we report a graphene-assisted vdW magnetic-electrode transfer technique that enables high-quality interfaces between different FM electrodes and various 2D materials. A monolayer graphene (MLG) is employed, not only to assist in peeling off the prepatterned FM electrodes from a sacrificial substrate, but also to serve as an inserting layer to modulate the contact resistance for optimizing spin injection. Based on the developed solvent-free magnetic-electrode transfer technique, atomically-smooth interfaces are achieved, enabling high-quality lateral spin valve devices equipped with gate electrodes for electrical tuning. We realize spin valves based on few-layer graphene (FLG), whose MR is among the best values reported in the literature. Further, we apply the technique to semiconducting MoS₂ to demonstrate transport of in-plane spins for ~ 1.4 μm and a maximum $|\text{MR}|$ as large as $\sim 20\%$, both of which are larger than previous results. According to our analysis, the tunneling interface resistance R_T is comparable with the spin

resistance of the channel R_{ch} in these devices, which is beneficial for spin injection. Finally, we show that the technique is applicable for realizing gate tunable spin valves based on fragile 2D organic/inorganic heterojunctions, and four-terminal spin valves for non-local spin detections. Our work unveils the powerful capability of FM electrode integrations using the developed vdW metal transfer technique, offering a promising future of 2D material-based spintronic applications.

Van der Waals magnetic-electrode transfer technique. Figure 1a shows the schematic of the device investigated in this work. It consists of a 2D spin transport channel (made of graphene, MoS₂, or 2D organic/inorganic heterojunctions) and two transferred FM electrodes (Fe₂₀Ni₈₀ and Co, respectively), serving as a two-terminal lateral spin valve. The FM electrodes are made of three layers of MLG, FM metal (Co or Fe₂₀Ni₈₀), and Au, which are deposited in sequence on a sacrificial substrate of SiO₂/Si. Taking advantage of the weak adhesion between MLG and SiO₂, the FM electrodes are easily peeled off from the sacrificial substrate, and then are placed onto different target 2D materials (see Figure 1b). It is worth noting that the MLG layer is detached from the substrate (see Figure 1c), which is different from the previously reported graphene-assisted metal transfer printing technology.²⁶ It protects FM metals from oxidation during the transfer process, and serves as part of the electrode to modulate the contact resistance for optimizing spin injection from FM metals to 2D materials. The vdW interaction between MLG and the target 2D material tends to result in a closely-attached interface, which is beneficial for spin injection and detection. Using this solvent-free technique, we can non-destructively place FM electrodes on various 2D materials to fabricate high-quality spin valve devices. More information can be found in Note S1 in Supporting Information.

The pristine quality of FM electrode/2D material interfaces is revealed by high-resolution transmission electron microscopy (TEM). Figure 1d (Figure 1f) shows a cross-sectional TEM image cutting underneath the Fe₂₀Ni₈₀ electrode, which is transferred onto FLG (MoS₂). The corresponding energy-dispersive x-ray spectroscopy (EDS) images are shown in Figure 2e (Figure 2g), from which an atomically-smooth interface between FM metal and FLG (MoS₂) is clearly resolved. No obvious diffusion of Ni and Fe atoms is found in the FLG (MoS₂) layer. Based on such damage-free interfaces, high-quality spin valve devices with effective spin injection are expected.

Graphene-based spin valves. Graphene has attracted significant research interests since its long l_{sf} and high carrier mobility are essential for spin transport.^{10, 14, 30} Figure 2a shows the cross-sectional schematic of the FLG-based device. A drain-source bias (V_{ds}) is applied between the two FM electrodes to generate a current of I_d to be measured. The heavily-doped Si substrate acts as a back gate where a voltage of V_{gs} can be applied (see Figure S2).

Figure 2b shows typical resistance curves when sweeping in-plane magnetic field at 1.5 K. Magnetizations of two FM electrodes (indicated by the arrows) flip as the field changes, resulting in different resistances. Here the MR ratio is defined as $MR = (R_H - R_P)/R_P$, where R_H is the magnetic field dependent resistance and R_P is the resistance corresponding to the parallel configuration. The measured $|MR|$ can be modulated by V_{ds} and V_{gs} , respectively (see Figure S3). As shown in Figure 2d, $|MR|$ reaches a maximum value of 8.6% at $V_{ds} = -0.1$ mV and decreases at higher $|V_{ds}|$, which can be understood as excitation of magnons, band bending, and involvement of interface states at high voltages.³¹ Meanwhile, as shown in Figure 2e, $|MR|$ exhibits a maximum value near the charge neutrality point at $V_{gs} = 0$ V (see the transfer characteristic curve shown in Figure S2b). Away from the charge neutrality point, the channel conductance σ_{ch} increases, while $|MR|$ decreases. This inverse scaling of MR with σ_{ch} is associated with spin injection process.³² According to the one-dimensional drift/diffusion theory of spin transport,³³ MR scales with $1/\sigma_{ch}$ for tunneling contacts, while scales with σ_{ch} for transparent contacts. Therefore, our results indicate that tunneling behavior is dominant at the contacts, which is consistent with the measured nonlinear I_d - V_{ds} curve (see Figure S2a) and the increased resistance at lower temperature (see Figure S4). This tunneling contact behavior is favorable for spin injection.

We use a standard drift/diffusion model^{34, 35} to estimate the spin polarization r_G at the FM electrode/FLG interface (see Note S2 in Supporting Information). Previous studies reveal that l_{sf} of FLG on SiO₂ substrate without any treatments is about several micrometers.³⁰ In this range, the spin polarization is estimated to be larger than 30% when $V_{ds} = -0.1$ mV (see Figure 2f). For comparison, a theoretical value of 33% is predicted in ideally lattice-matched FM metal/MLG/FM metal structures, resulting from the K-point spin filtering mechanism.³⁶ This suggests that the non-destructive vdW magnetic-electrode transfer technique provides an ideal spin injection interface.

More importantly, we investigate the spin valve effect at elevated temperature and observe that $|MR|$ persists up to 300 K (see Figure 2c). As shown in Figure 2g, we benchmark our data with previous results,^{1, 35, 37-41} obtained from similar two-terminal lateral spin valves based on FLG. A

trend of $|\text{MR}|$ decrease with increased temperature is observed, which can be explained by the spin wave excitation model.⁴² It is demonstrated that $|\text{MR}|$ of our devices are among the best values at most of temperature ranges. This indicates the powerful capability of the developed technique in achieving effective spin polarization.

MoS₂-based spin valves. The intrinsic spin-orbit coupling in monolayer semiconducting MoS₂ offers a powerful knob for electrical control of spins.^{14, 43} However, it also leads to quick relaxation of in-plane spins due to the D'yakonov-Perel' (DP) mechanism.^{44, 45} Previous studies have suggested that transition metal dichalcogenides with even layers recover the inversion symmetry, effectively suppressing the DP spin relaxation.¹³ As a consequence, lateral spin valves based on even-layer MoS₂ are expected to carry spins with slower spin relaxation and longer l_{sf} .

Here, we investigate devices based on bilayer MoS₂ (see Figure 3a) and focus on their performance at low temperature. From the dc transfer curve (see Figure S5a), the two-terminal field-effect mobility is estimated to be $\sim 30 \text{ cm}^2\text{V}^{-1}\text{s}^{-1}$ at 0.3 K. The relatively low value is probably due to tunneling-dominant behaviors at the contacts, which is revealed by the quasi-symmetric nonlinearity in output curves (see Figure S5b). Then we use the lock-in technique to study spin transport behaviors. As shown in Figures 3b and 3c, pronounced spin valve effect is observed, which can be strongly modulated by gate voltage V_{gs} . Figure 3d shows maximum measurable $|\text{MR}|$ as a function of V_{gs} . It increases first and then decreases, reaching a maximum value of 22.1% at $V_{\text{gs}} = 34 \text{ V}$.

This behavior is similar to the previous observation, which is understood as manipulating the ratio between R_{T} and R_{ch} (Ref. 13). Figure 3e shows calculated MR as a function of $R_{\text{T}}/R_{\text{ch}}$ based on Equation S1 and experimental parameters. MR reaches its maximum when $R_{\text{T}} \approx R_{\text{ch}}$, which corresponds to a perfect balance between the spin injection rate and the spin relaxation rate. A larger R_{T} decreases the spin injection rate, while a larger R_{ch} induces a spin-backflow process causing the relaxation of spin within the FM electrodes. In MoS₂ devices, R_{T} is affected by the Schottky barriers at the contacts, and R_{ch} depends on the resistivity ρ thus the carrier density as well as the mobility. All of these parameters are modulated by V_{gs} (see Figure S5). Therefore, MR exhibits a peak upon varying V_{gs} . Based on this physical picture, R_{T} is estimated to be comparable with R_{ch} at $V_{\text{gs}} = 34 \text{ V}$. Assuming $R_{\text{T}}=R_{\text{ch}}$, we obtain $\rho \sim 10^5 \Omega$ in our bilayer MoS₂ devices, which is consistent with reported values at low temperature.¹³

It is worth noting that the peak $|\text{MR}|$ of our device is as large as $\sim 20\%$, which is much larger than $\sim 1\%$ reported in Ref. 13. Using a similar way, we roughly estimate that l_{sf} in our device is as large as $1.25 \mu\text{m}$, which is about 5 times larger than the previous result.¹³ This increase may result from the solvent-free feature of the technique developed in this work, since exposing 2D materials to solvents is demonstrated to cause additional spin scattering.⁴⁶ Indeed, we observe clear spin valve effect in an additional MoS_2 device with a channel length of $\sim 1.4 \mu\text{m}$ (see Figure S6). Our results suggest in-plane spins can transport over a microscale distance in bilayer MoS_2 , offering a promising future of gate-tunable spintronic devices based on semiconducting MoS_2 .

Theoretical analysis of FLG- and MoS_2 -based devices. According to our drift/diffusion model, r_G is estimated to be $\sim 30\%$. However, such a value cannot account for the large $|\text{MR}|$ measured in MoS_2 -based devices, no matter what l_{sf} of MoS_2 is chosen. This strongly hints at a larger spin polarization r_M at the FM electrode/ MoS_2 interface (similar to Ref. 13, we use $r_M=50\%$ for obtaining Figure 3e, which corresponds to the maximum spin polarization of $\text{Fe}_{20}\text{Ni}_{80}$). To better understand this, we perform density functional theory (DFT) calculations for Fe-Ni/MLG/FLG and Fe-Ni/MLG/2L- MoS_2 stacks (see Figures 4a and 4b, respectively). Note that maximum $|\text{MR}|$ of FLG-based devices (8.6%) appears at $V_{\text{gs}}=0 \text{ V}$, while $|\text{MR}|$ of MoS_2 -based devices peaks (22.1%) at $V_{\text{gs}}=34 \text{ V}$ (corresponding to an electron density of $3 \times 10^{12} \text{ cm}^{-2}$). Therefore, we calculate spin-dependent densities of state (DOSs) of FLG- and MoS_2 -based stacks at both pristine case and at the doping level of $n_s=3 \times 10^{12} \text{ cm}^{-2}$ (see Figures 4c and 4d, respectively). Spin polarizations at the interfaces are estimated¹⁹ as $P_{G/M} = \frac{n_{\uparrow}-n_{\downarrow}}{n_{\uparrow}+n_{\downarrow}}$, where G (M) represents FLG (MoS_2), and n_{\uparrow} (n_{\downarrow}) is the spin-up (spin-down) DOS at the Fermi level (dashed lines in Figures 4c and 4d). Although for the pristine case, P_G is almost equal to P_M , their difference increases dramatically upon electrical doping. This is because that the semiconducting nature of MoS_2 enables effective tuning of the Fermi level, while the gating effect of FLG is rather limited. As a result, P_M ($n_s=3 \times 10^{12} \text{ cm}^{-2}$) is larger than P_G (pristine) under the experimental conditions (see Figure 4e), which agrees well with a larger r_M estimated from our drift/diffusion model qualitatively. We believe this is the main reason for the larger $|\text{MR}|$ found in our MoS_2 -based devices.

In addition to modulating the interface spin polarization, the gating effect also strongly manipulates R_T/R_{ch} in semiconducting MoS_2 (as discussed in Figure 3e), while has limited influence in FLG. We can calculate R_T and R_{ch} in our FLG-based devices to examine the ratio of

R_T/R_{ch} based on Equation S1 and parameters of $\rho \sim 589 \text{ } \Omega$ (measured from an additional four-terminal device as shown in our previous work²⁸), $r_G \sim 30\%$, and $l_{sf} \sim 9 \text{ } \mu\text{m}$ (determined by the measured $|\text{MR}| = 8.6\%$ from Figure 2f). Interestingly, R_T is found to be comparable with R_{ch} in our FLG-based devices (see the blue hexagon in Figure 4f), even if variations in r_G are considered (see Figure S7). This good conductance match also contributes to large $|\text{MR}|$ in our FLG-based devices, as benchmarked in Figure 2g.

Finally, we would like to briefly comment on the role of MLG as an inserting layer for optimizing the spin injection, although it has been debated for more than a decade and is still not fully understood.^{19, 36, 47-53} Besides the intuitive idea of using the large out-of-plane resistance of graphene to serve as a tunneling layer, theoretical proposals illustrate that matching spin-polarized bands in FM metals and the electronic states in MLG results in a phenomenon known as “K-point spin filtering”.^{36, 53} Recently, it is demonstrated that the proximity effect cannot be neglected, which results in strong interfacial hybridization between MLG and the FM metal¹⁹ accounting for a larger measured MR. In addition, metal-induced doping and exchange-proximity induced spin polarization in MLG also contribute to the spin injection.⁵⁰ In our devices, although experimental evidence hints at pronounced tunneling and good conductance match at the contacts, DFT calculations suggest interfacial hybridization is also relevant (see Figures 4a and 4b). Further experiments can be expected on nanojunctions realized by transferring our multilayer magnetic-electrodes onto monocrystalline FM metals with controlled twist angles¹⁹ to investigate the two aforementioned mechanisms in more details. Nevertheless, our results demonstrate the developed graphene-assisted vdW magnetic-electrode transfer technique is powerful for obtaining high-quality FM electrode/2D material interfaces, which are responsible for effective spin injection.

Spin valves based on 2D organic/inorganic heterojunctions. Spins in 2D organic materials are expected to have long life time due to the relatively weak spin-orbit coupling and hyperfine interaction.^{54, 55} However, they are fragile and are easily damaged during conventional fabrication processes. Using the developed technique, we are able to realize gate-tunable spin valve devices based on the heterojunction of bilayer C₈-BTBT and FLG (see Figure 5a). The FLG flake not only acts as the substrate for synthesizing the organic C₈-BTBT crystal, but also serves as a spin transport channel. Beyond our previous work²⁸, we demonstrate MR can be tuned upon varying V_{gs} (see Figure 5b). We would like to point out that a symmetric sign inversion of MR is observed

when the polarity of V_{ds} is changed in our devices²⁸ (see Figure S8), which is different from previous reports.⁵⁶⁻⁵⁹ The physical mechanism is not understood yet which invites further investigations.

Four-terminal spin valve devices. Besides the investigated two-terminal spin valve devices, the developed vdW magnetic-electrode transfer technique is also applicable for four-terminal devices. By sequentially transferring electrodes onto a chosen FLG flake, four-terminal devices can be fabricated (see Figure 5c), allowing non-local investigations of spin transport. Here, we use the standard lock-in technique to measure the non-local resistance ΔR_{NL} (see Figure S9). Figure 5d shows ΔR_{NL} as a function of bias current I_{dc} , showing a decrease as I_{dc} changes from -100 μA to 100 μA . This can be attributed to the electric field-induced spin drift in the spin injection channel.⁶⁰
⁶¹ In addition, we observe $\Delta R_{NL} \sim 0.04 \Omega$ in an additional device (see Figure S10).

In conclusion, we report a graphene-assisted magnetic-electrode transfer technique that enables spin valve devices with atomically-smooth and damage-free interfaces between FM metals and various 2D materials. These include FLG devices that exhibit $|MR|$ which is among the best values in the literature, MoS₂ devices with a record high $|MR|$ of $\sim 20\%$ and an in-plane spin transport distance of $\sim 1.4 \mu m$, and hybrid devices based on 2D organic/inorganic heterojunctions that enable gate control on MR. We also demonstrate that the technique is applicable for four-terminal spin valves allowing non-local measurements. The developed solvent-free technique prevents 2D spin transport channel from contacting with solvents, which suppresses spin dephasing resulting from contaminations by solvents.⁴⁶ Making use of the diversity of 2D organic^{59, 62-64}, inorganic materials^{2, 6, 14, 65} and their heterojunctions,^{66, 67} our work provides a promising future of employing the vdW metal transfer technique for advanced 2D spintronic applications.

ASSOCIATED CONTENT

Supporting Information. The Supporting Information is available free of charge at XXXXX.

Experimental methods, estimation of spin polarization in FLG-based devices, transfer and output characteristic curves of the devices in the main text, additional MR curves including those from additional devices, details of data points used for benchmarking, and calculation of R_T/R_{ch} for FLG-based devices.

AUTHOR INFORMATION

Corresponding Author

*Email: (W.Q.) wqin@sdu.edu.cn.

*Email: (Y.X.) xuyong@njupt.edu.cn.

*Email: (Q.Z.) iamqzhao@njupt.edu.cn.

*Email: (X.-X.S.) songxx90@ustc.edu.cn.

Author Contributions

Z.L. and X.-X.S. conceived the project. Z.L. and X.-X.S. designed the experiment. Z.L., Z.Y., Y.Yu, Y.Yao, C.L.T., H.S., L.G., Y.X., Q.Z., and X.-X.S. contributed to sample preparation, characterization, device fabrication, measurements, and data analysis. Z.L. W.N. and F.T. prepared the TEM specimens. X.L and W.Q. carried out the DFT calculations. Z.L. and X.-X.S. cowrote the manuscript with inputs from other authors. All authors contributed to discussions.

Notes

The Authors declare no conflict of interest.

ACKNOWLEDGMENT

We would like to thank Xinran Wang (Nanjing University), Guoping Guo (University of Science and Technology of China) and Wei Han (Peking University) for the support in this work. The authors acknowledge support from the Natural Science Foundation of Jiangsu Province (Grant No. BK20220397), the National Natural Science Foundation of China (Grant Nos. 62204130, 12274397), the National Funds for Distinguished Young Scientists (Grant No. 61825503), the Natural Science Foundation of the Higher Education Institutions of Jiangsu Province (Grant No.

22KJB510010), the Science Foundation of Nanjing University of Posts and Telecommunications (Grant No. NY221116), Guangdong Province Research and Development in Key Fields from Guangdong Greater Bay Area Institute of Integrated Circuit and System (No. 2021B0101280002) and Guangzhou City Research and Development Program in Key Field (No. 20210302001)

Figures:

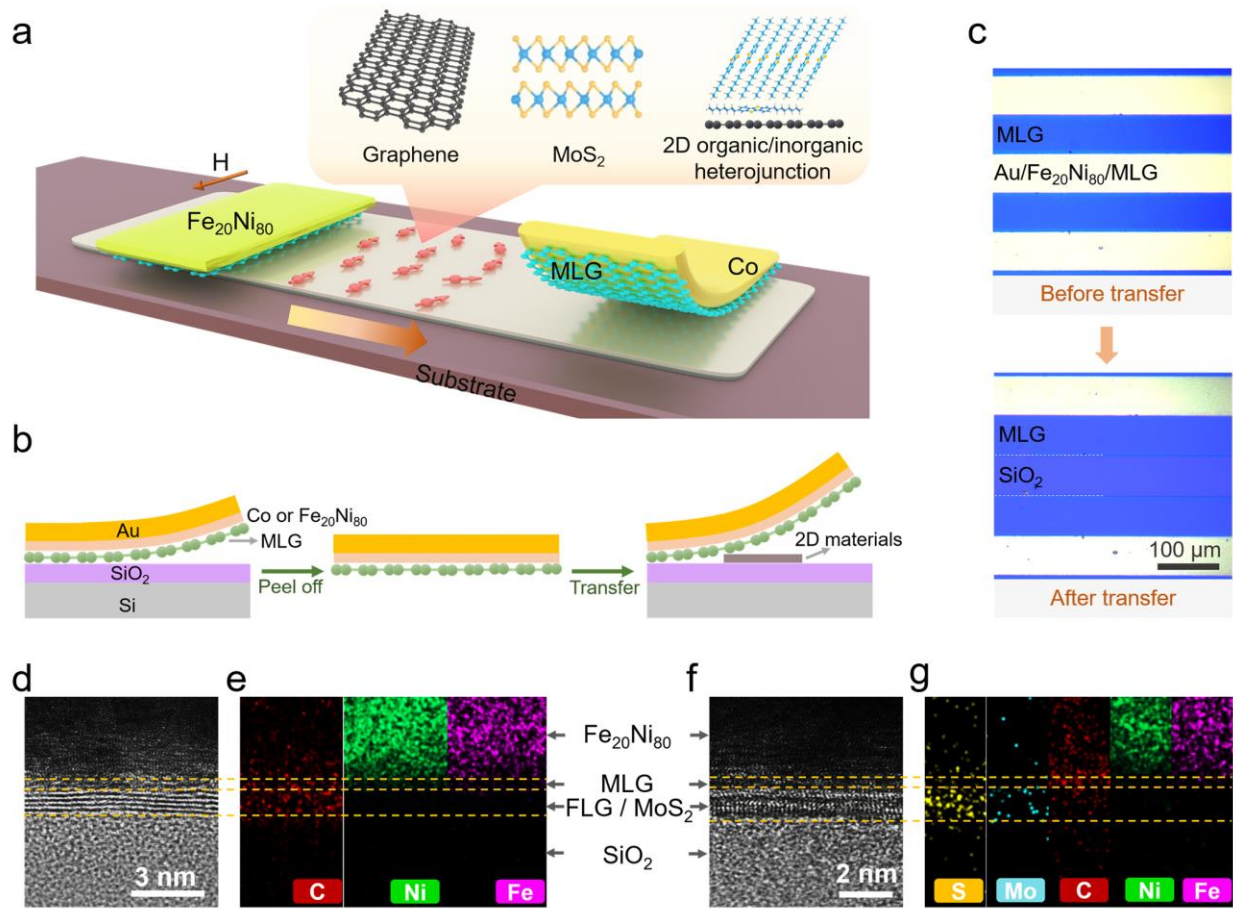


Figure 1. a) Schematic of a lateral spin valve device consisting of a 2D spin transport channel (made of graphene, MoS₂, or 2D organic/inorganic heterojunctions) and two transferred FM electrodes (Fe₂₀Ni₈₀ and Co, respectively). b) Schematic of the graphene-assisted vdW magnetic-electrode transfer technique for FM electrode integrations. c) Optical images of multilayer FM electrodes on the sacrificial substrate before (top) and after (bottom) electrode transfer. Edges (white dotted lines) between MLG and exposed SiO₂ surface indicate that MLG is detached from the sacrificial substrate and serves as part of the multilayer FM electrode. d) Cross-sectional TEM image cutting underneath the Fe₂₀Ni₈₀ electrode which is transferred onto FLG and e) the corresponding elemental mappings. f) Cross-sectional TEM image cutting underneath the Fe₂₀Ni₈₀ electrode which is transferred onto MoS₂ and g) the corresponding elemental mappings.

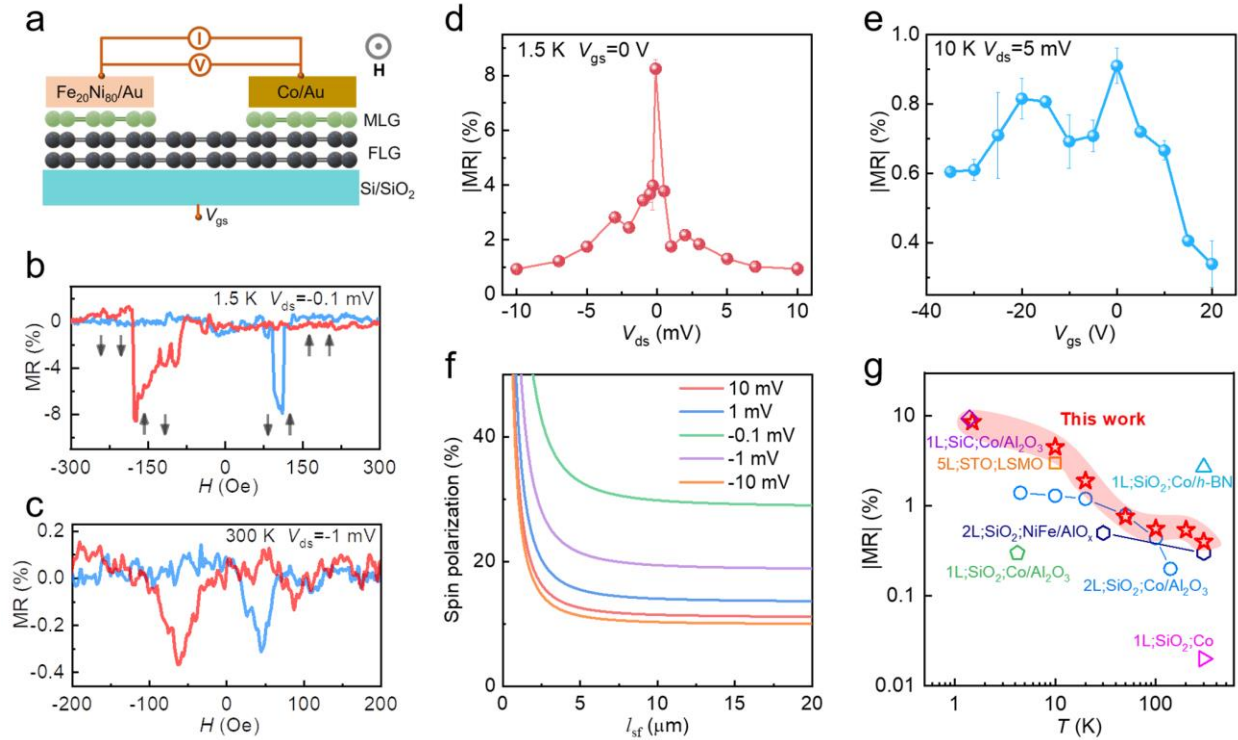


Figure 2. a) Schematic of a two-terminal lateral FLG-based spin valve with transferred FM electrodes. MR curves measured b) at 1.5 K, $V_{ds} = -0.1$ mV, and c) at 300 K, $V_{ds} = -1$ mV, respectively. Arrows indicate magnetizations of two FM electrodes. Extracted maximum measurable $|MR|$ as functions of d) bias voltage, and e) gate voltage, respectively. f) Calculated spin polarization at different l_{sf} based on Equation S1. Each curve corresponds to the data obtained at a fixed V_{ds} shown in d). g) Benchmarking of $|MR|$ as a function of temperature with results obtained from similar two-terminal lateral spin valves based on FLG reported in the literature. Labels mark the thickness of graphene, the substrate, and the FM electrode. Details of data points are presented in Table S1.

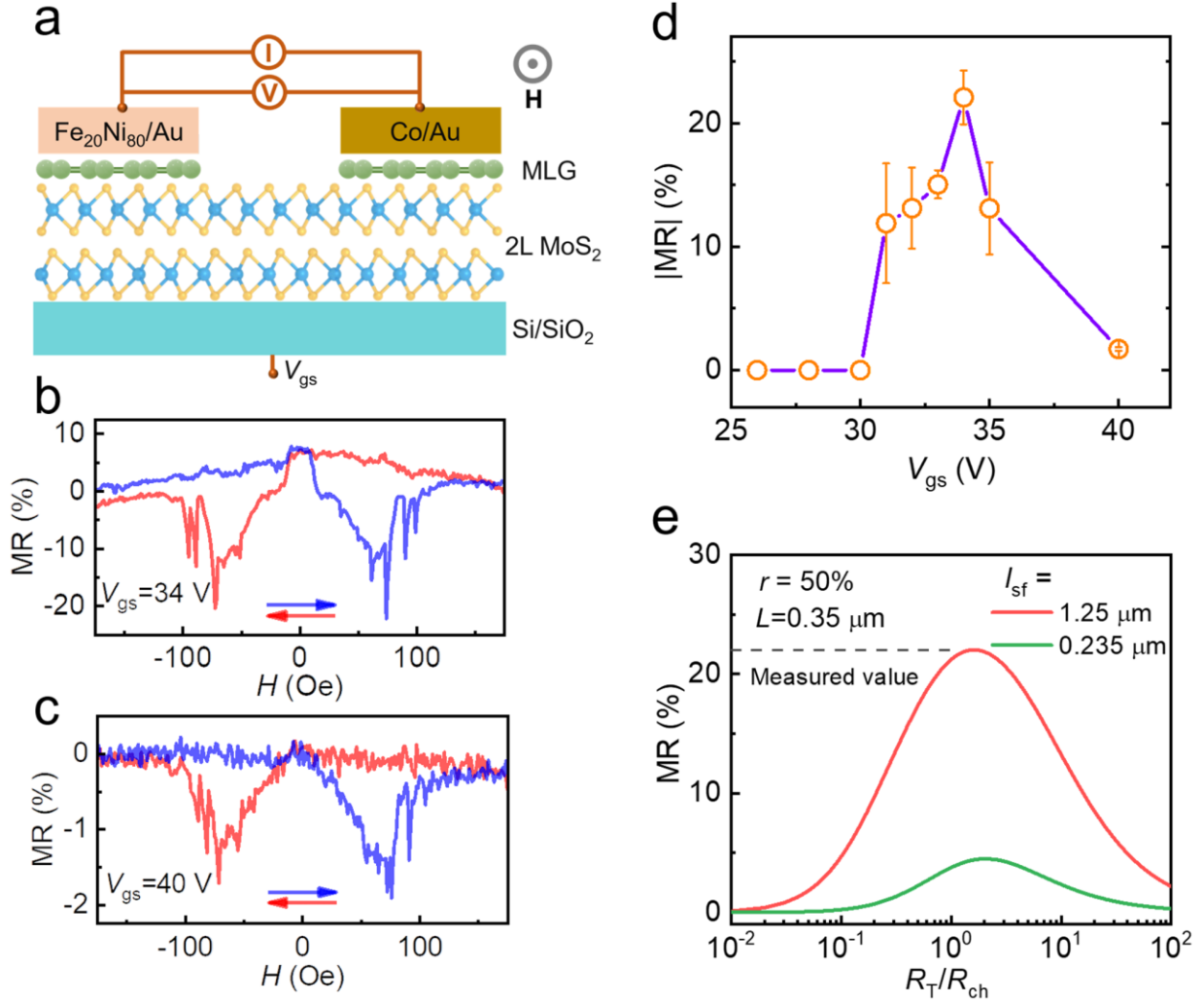


Figure 3. a) Schematic of a two-terminal lateral MoS₂-based spin valve with transferred FM electrodes. MR curves measured at 0.3 K, $V_{ds} = -2$ mV, with b) $V_{gs} = 34$ V, and c) $V_{gs} = 40$ V, respectively. Arrows indicate sweeping directions of the magnetic field. The channel length and width of the tested device are 0.35 μm and 4.6 μm , respectively. d) Extracted maximum measurable $|\text{MR}|$ as a function of gate voltage. e) Calculated MR as a function of R_T/R_{ch} based on Equation S1. Assuming the interface spin polarization of $\sim 50\%$ (Ref. 13), corresponding to the maximum spin polarization of Fe₂₀Ni₈₀, $l_{sf}=1.25$ μm is needed to reproduce the measured maximum $|\text{MR}|$ of 22.1% (red curve). For comparison, the green curve corresponds to the calculated result based on $l_{sf}=0.235$ μm reported previously (Ref. 13).

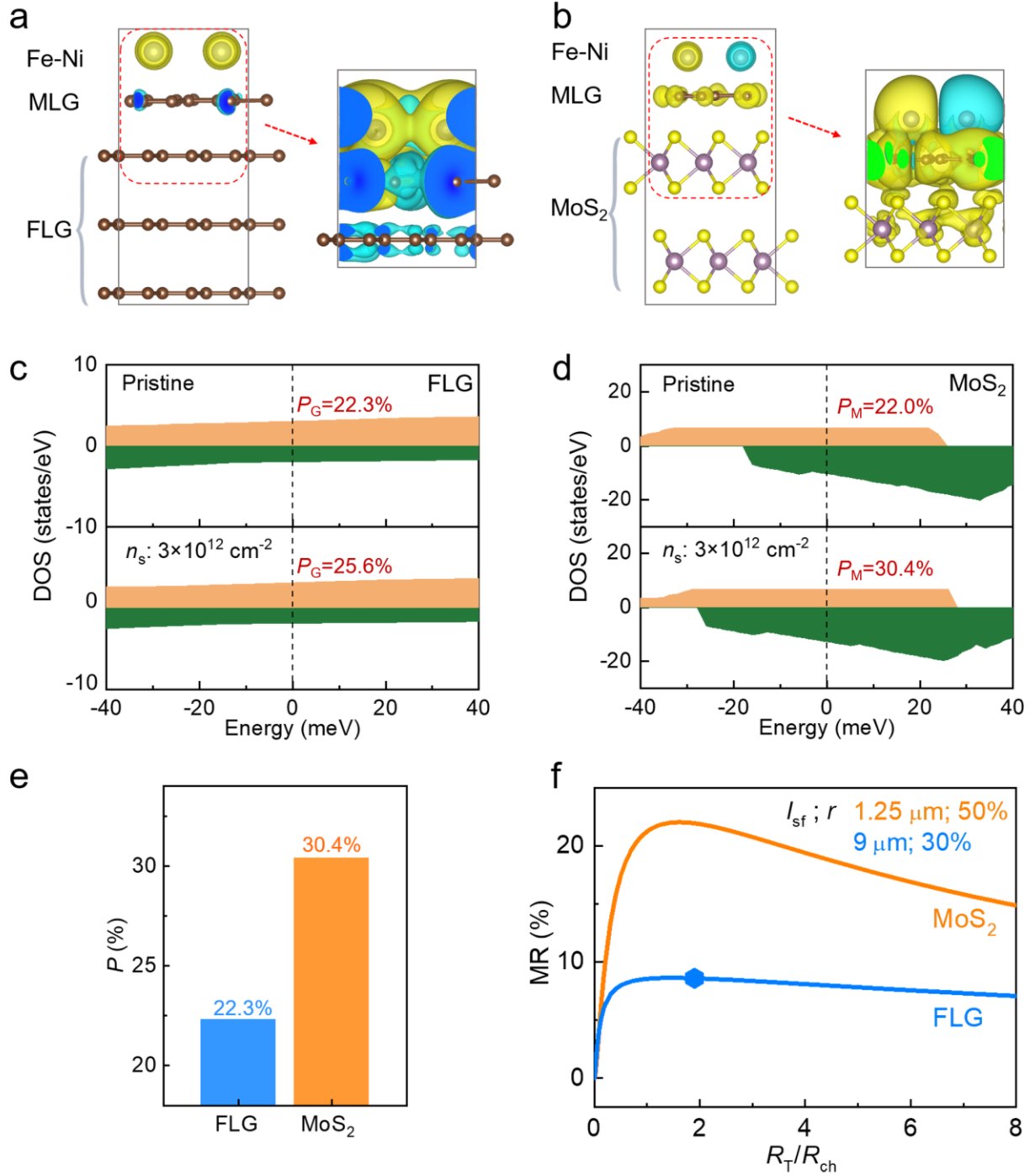


Figure 4. Schematic illustration of a) Fe-Ni/MLG/FLG and b) Fe-Ni/MLG/2L-MoS₂ stacks for DFT calculations, respectively. The black boxes mark the unit cell used in DFT calculations, which are overlaid by the spin dependent charge density distributions (cyan and yellow represent spin up and spin down, respectively). The right panels in a) and b) are zoom-in images of the red dashed boxes, highlighting spin dependent charge density distributions near interfaces. Calculated spin

dependent DOSs for c) Fe-Ni/MLG/FLG and d) Fe-Ni/MLG/2L-MoS₂ stacks, respectively. The upper panels in c) and d) correspond to the scenario without additional electrons induced (referred to as pristine), while the bottom panels pertain to the condition where an additional electron density of $n_s=3\times 10^{12}$ cm⁻² is introduced. P_G (P_M) represents calculated interface spin polarization for the FLG-based (MoS₂-based) stack. e) Calculated P_G (pristine) and P_M ($n_s=3\times 10^{12}$ cm⁻²) under the experimental conditions, showing a clear difference. f) Calculated MR as a function of R_T/R_{ch} for FLG-based (blue) and MoS₂-based devices (orange) using Equation S1, respectively. The blue hexagon marks the working point of R_T/R_{ch} , which is calculated based on experimental parameters.

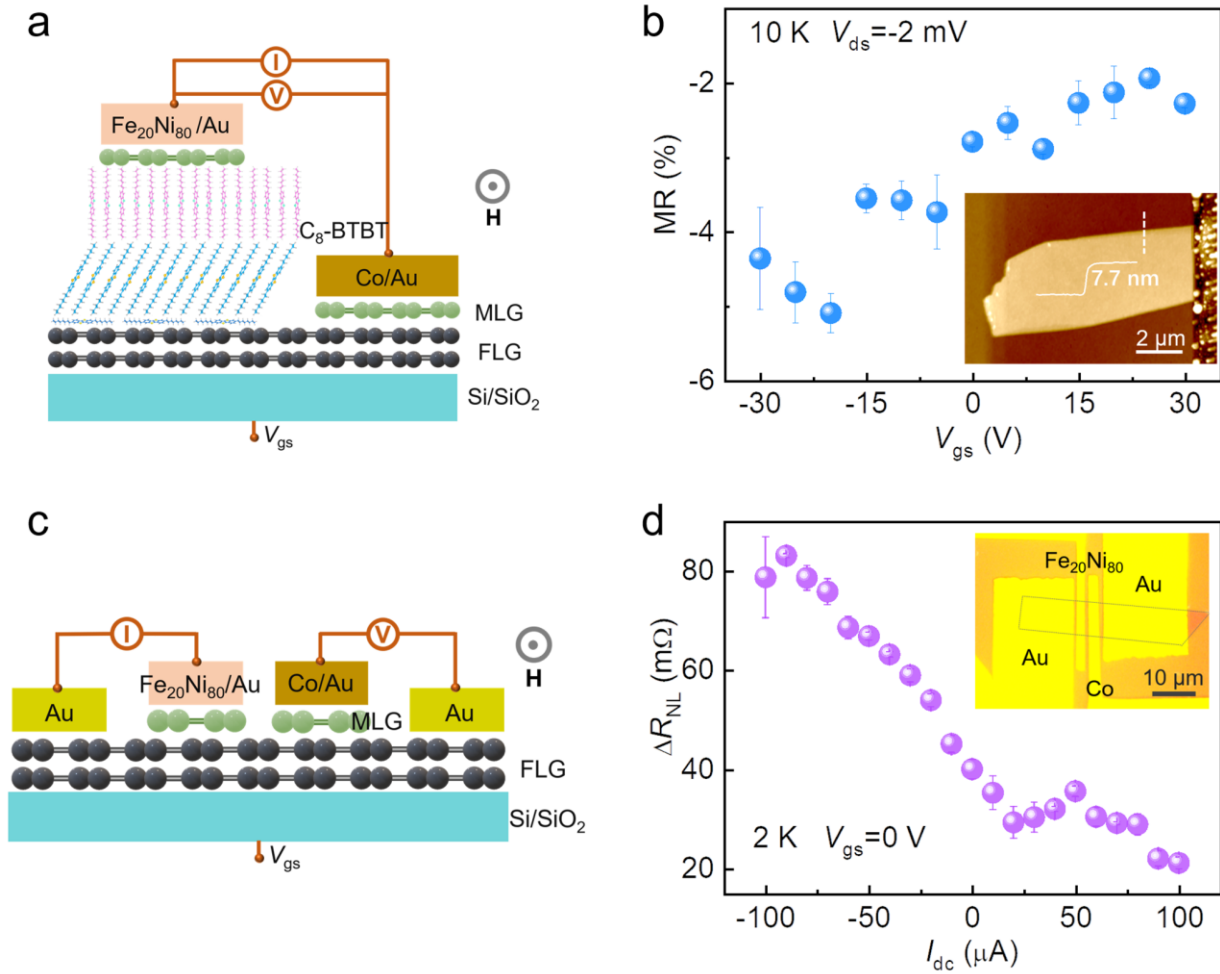


Figure 5. a) Schematic of a two-terminal hybrid spin valve based on 2D organic/inorganic heterojunction, where transferred FM electrodes are used for spin injection and detection. b) Extracted maximum measurable MR as a function of V_{gs} obtained at V_{ds} of -2 mV. The data are collected at 10 K. Inset shows an AFM image of the heterojunction of bilayer C_8 -BTBT and FLG with the total thickness of ~ 7.7 nm. c) Schematic of a four-terminal FLG-based spin valve with corresponding optical image shown in the inset of d). Gray dotted lines highlight edges of the FLG channel. The device has two inner FM electrodes ($Fe_{20}Ni_{80}$ (2 μm in width) and Co (2.5 μm in width), respectively) and two outer non-magnetic electrodes. d) Non-local resistance ΔR_{NL} as a function of I_{dc} measured at 2 K.

REFERENCES

- (1) Tombros, N.; Jozsa, C.; Popinciuc, M.; Jonkman, H. T.; van Wees, B. J. Electronic spin transport and spin precession in single graphene layers at room temperature. *Nature* **2007**, *448*, 571-574.
- (2) Yang, H.; Valenzuela, S. O.; Chshiev, M.; Couet, S.; Dieny, B.; Dlubak, B.; Fert, A.; Garello, K.; Jamet, M.; Jeong, D.-E.; et al. Two-dimensional materials prospects for non-volatile spintronic memories. *Nature* **2022**, *606*, 663-673.
- (3) Song, T.; Cai, X.; Tu, M. W.-Y.; Zhang, X.; Huang, B.; Wilson, N. P.; Seyler, K. L.; Zhu, L.; Taniguchi, T.; Watanabe, K.; et al. Giant tunneling magnetoresistance in spin-filter van der Waals heterostructures. *Science* **2018**, *360*, 1214-1218.
- (4) Lin, X.; Yang, W.; Wang, K. L.; Zhao, W. Two-dimensional spintronics for low-power electronics. *Nature Electronics* **2019**, *2*, 274-283.
- (5) Zhao, B.; Ngalyo, R.; Ghosh, S.; Ershadrad, S.; Gupta, R.; Ali, K.; Hoque, A. M.; Karpiak, B.; Khokhriakov, D.; Polley, C.; et al. A Room-Temperature Spin-Valve with van der Waals Ferromagnet Fe₅GeTe₂/Graphene Heterostructure. *Advanced Materials* **2023**, *35*, 2209113.
- (6) Avsar, A.; Tan, J. Y.; Kurpas, M.; Gmitra, M.; Watanabe, K.; Taniguchi, T.; Fabian, J.; Özyilmaz, B. Gate-tunable black phosphorus spin valve with nanosecond spin lifetimes. *Nature Physics* **2017**, *13*, 888-893.
- (7) Sierra, J. F.; Fabian, J.; Kawakami, R. K.; Roche, S.; Valenzuela, S. O. Van der Waals heterostructures for spintronics and opto-spintronics. *Nature Nanotechnology* **2021**, *16*, 856-868.
- (8) Wang, Z.; Zhang, T.; Ding, M.; Dong, B.; Li, Y.; Chen, M.; Li, X.; Huang, J.; Wang, H.; Zhao, X.; et al. Electric-field control of magnetism in a few-layered van der Waals ferromagnetic semiconductor. *Nature Nanotechnology* **2018**, *13*, 554-559.
- (9) Bisswanger, T.; Winter, Z.; Schmidt, A.; Volmer, F.; Watanabe, K.; Taniguchi, T.; Stampfer, C.; Beschoten, B. CVD Bilayer Graphene Spin Valves with 26 μm Spin Diffusion Length at Room Temperature. *Nano Letters* **2022**, *22*, 4949-4955.
- (10) Ghising, P.; Biswas, C.; Lee, Y. H. Graphene Spin Valves for Spin Logic Devices. *Advanced Materials* **2023**, *35*, 2209137.
- (11) Panda, J.; Ramu, M.; Karis, O.; Sarkar, T.; Kamalakar, M. V. Ultimate Spin Currents in Commercial Chemical Vapor Deposited Graphene. *ACS Nano* **2020**, *14*, 12771-12780.
- (12) Dankert, A.; Dash, S. P. Electrical gate control of spin current in van der Waals heterostructures at room temperature. *Nature Communications* **2017**, *8*, 16093.
- (13) Liang, S.; Yang, H.; Renucci, P.; Tao, B.; Laczkowski, P.; Mc-Murtry, S.; Wang, G.; Marie, X.; George, J.-M.; Petit-Watelot, S.; et al. Electrical spin injection and detection in molybdenum disulfide multilayer channel. *Nature Communications* **2017**, *8*, 14947.
- (14) Avsar, A.; Ochoa, H.; Guinea, F.; Özyilmaz, B.; van Wees, B. J.; Vera-Marun, I. J. Colloquium: Spintronics in graphene and other two-dimensional materials. *Rev. Mod. Phys.* **2020**, *92*, 021003.
- (15) Galbiati, M.; Tatay, S.; Dubois, S. M. M.; Godel, F.; Galceran, R.; Mañas-Valero, S.; Piquemal-Banci, M.; Vecchiola, A.; Charlier, J.-C.; Forment-Aliaga, A.; et al. Path to Overcome Material and Fundamental Obstacles in Spin Valves Based on MoS₂ and Other Transition-Metal Dichalcogenides. *Physical Review Applied* **2019**, *12*, 044022.
- (16) Wang, S.-J.; Venkateshvaran, D.; Mahani, M. R.; Chopra, U.; McNellis, E. R.; Di Pietro, R.; Schott, S.; Wittmann, A.; Schweicher, G.; Cubukcu, M.; et al. Long spin diffusion lengths in

- doped conjugated polymers due to enhanced exchange coupling. *Nature Electronics* **2019**, *2*, 98-107.
- (17) Li, D.; Yu, G. Innovation of Materials, Devices, and Functionalized Interfaces in Organic Spintronics. *Advanced Functional Materials* **2021**, *31*, 2100550.
- (18) Hu, S.; Liu, W.; Guo, L.; Zhang, R.; Gu, X.; Meng, K.; Qin, Y.; Guo, A.; Yang, T.; Zhang, C.; et al. Continuous Room-Temperature Spin-Injection Modulation Achieved by Spin-Filtering Competition in Molecular Spin Valves. *Advanced Materials* **2023**, *35*, 2300055.
- (19) Piquemal-Banci, M.; Galceran, R.; Dubois, S. M. M.; Zatzko, V.; Galbiati, M.; Godel, F.; Martin, M.-B.; Weatherup, R. S.; Petroff, F.; Fert, A.; et al. Spin filtering by proximity effects at hybridized interfaces in spin-valves with 2D graphene barriers. *Nature Communications* **2020**, *11*, 5670.
- (20) Dayen, J.-F.; Ray, S. J.; Karis, O.; Vera-Marun, I. J.; Kamalakar, M. V. Two-dimensional van der Waals spinterfaces and magnetic-interfaces. *Applied Physics Reviews* **2020**, *7*, 011303.
- (21) Wang, W.; Narayan, A.; Tang, L.; Dolui, K.; Liu, Y.; Yuan, X.; Jin, Y.; Wu, Y.; Rungger, I.; Sanvito, S.; et al. Spin-Valve Effect in NiFe/MoS₂/NiFe Junctions. *Nano Letters* **2015**, *15*, 5261-5267.
- (22) Liu, Y.; Guo, J.; Zhu, E.; Liao, L.; Lee, S.-J.; Ding, M.; Shakir, I.; Gambin, V.; Huang, Y.; Duan, X. Approaching the Schottky–Mott limit in van der Waals metal–semiconductor junctions. *Nature* **2018**, *557*, 696-700.
- (23) Allain, A.; Kang, J.; Banerjee, K.; Kis, A. Electrical contacts to two-dimensional semiconductors. *Nature Materials* **2015**, *14*, 1195-1205.
- (24) Tang, Q.; Tong, Y.; Li, H.; Ji, Z.; Li, L.; Hu, W.; Liu, Y.; Zhu, D. High-Performance Air-Stable Bipolar Field-Effect Transistors of Organic Single-Crystalline Ribbons with an Air-Gap Dielectric. *Advanced Materials* **2008**, *20*, 1511-1515.
- (25) Luo, Z.; Peng, B.; Zeng, J.; Yu, Z.; Zhao, Y.; Xie, J.; Lan, R.; Ma, Z.; Pan, L.; Cao, K.; et al. Sub-thermionic, ultra-high-gain organic transistors and circuits. *Nature Communications* **2021**, *12*, 1928.
- (26) Liu, G.; Tian, Z.; Yang, Z.; Xue, Z.; Zhang, M.; Hu, X.; Wang, Y.; Yang, Y.; Chu, P. K.; Mei, Y.; et al. Graphene-assisted metal transfer printing for wafer-scale integration of metal electrodes and two-dimensional materials. *Nature Electronics* **2022**, *5*, 275-280.
- (27) Qi, D.; Li, P.; Ou, H.; Wu, D.; Lian, W.; Wang, Z.; Ouyang, F.; Chai, Y.; Zhang, W. Graphene-Enhanced Metal Transfer Printing for Strong van der Waals Contacts between 3D Metals and 2D Semiconductors. *Advanced Functional Materials* **2023**, *n/a*, 2301704.
- (28) Luo, Z.; Song, X.; Liu, X.; Lu, X.; Yao, Y.; Zeng, J.; Li, Y.; He, D.; Zhao, H.; Gao, L.; et al. Revealing the key role of molecular packing on interface spin polarization at two-dimensional limit in spintronic devices. *Science Advances* **2023**, *9*, eade9126.
- (29) Ding, S.; Tian, Y.; Wang, H.; Zhou, Z.; Mi, W.; Ni, Z.; Zou, Y.; Dong, H.; Gao, H.; Zhu, D.; et al. Reliable Spin Valves of Conjugated Polymer Based on Mechanically Transferrable Top Electrodes. *ACS Nano* **2018**, *12*, 12657-12664.
- (30) Han, W.; Kawakami, R. K.; Gmitra, M.; Fabian, J. Graphene spintronics. *Nature Nanotechnology* **2014**, *9*, 794-807.
- (31) Moodera, J. S.; Nowak, J.; van de Veerdonk, R. J. M. Interface Magnetism and Spin Wave Scattering in Ferromagnet-Insulator-Ferromagnet Tunnel Junctions. *Physical Review Letters* **1998**, *80*, 2941-2944.

- (32) Han, W.; Pi, K.; McCreary, K. M.; Li, Y.; Wong, J. J. I.; Swartz, A. G.; Kawakami, R. K. Tunneling Spin Injection into Single Layer Graphene. *Physical Review Letters* **2010**, *105*, 167202.
- (33) Takahashi, S.; Maekawa, S. Spin injection and detection in magnetic nanostructures. *Physical Review B* **2003**, *67*, 052409.
- (34) Jaffrès, H.; George, J. M.; Fert, A. Spin transport in multiterminal devices: Large spin signals in devices with confined geometry. *Physical Review B* **2010**, *82*, 140408.
- (35) Dlubak, B.; Martin, M.-B.; Deranlot, C.; Servet, B.; Xavier, S.; Mattana, R.; Sprinkle, M.; Berger, C.; De Heer, W. A.; Petroff, F.; et al. Highly efficient spin transport in epitaxial graphene on SiC. *Nature Physics* **2012**, *8*, 557-561.
- (36) Karpan, V. M.; Giovannetti, G.; Khomyakov, P. A.; Talanana, M.; Starikov, A. A.; Zwierzycki, M.; van den Brink, J.; Brocks, G.; Kelly, P. J. Graphite and Graphene as Perfect Spin Filters. *Physical Review Letters* **2007**, *99*, 176602.
- (37) Yan, W.; Phillips, L. C.; Barbone, M.; Hämmäläinen, S. J.; Lombardo, A.; Ghidini, M.; Moya, X.; Maccherozzi, F.; van Dijken, S.; Dhessi, S. S.; et al. Long Spin Diffusion Length in Few-Layer Graphene Flakes. *Physical Review Letters* **2016**, *117*, 147201.
- (38) Gurrum, M.; Omar, S.; Wees, B. J. v. Bias induced up to 100% spin-injection and detection polarizations in ferromagnet/bilayer-hBN/graphene/hBN heterostructures. *Nature Communications* **2017**, *8*, 248.
- (39) Shiraishi, M.; Ohishi, M.; Nouchi, R.; Mitoma, N.; Nozaki, T.; Shinjo, T.; Suzuki, Y. Robustness of Spin Polarization in Graphene-Based Spin Valves. *Advanced Functional Materials* **2009**, *19*, 3711-3716.
- (40) Ghiasi, T. S.; Kaverzin, A. A.; Dismukes, A. H.; de Wal, D. K.; Roy, X.; van Wees, B. J. Electrical and thermal generation of spin currents by magnetic bilayer graphene. *Nature Nanotechnology* **2021**, *16*, 788-794.
- (41) Afzal, A. M.; Khan, M. F.; Eom, J. Gate-Voltage-Modulated Spin Precession in Graphene/WS₂ Field-Effect Transistors. *Electronics*, **2021**, *10*, 2879.
- (42) Shang, C. H.; Nowak, J.; Jansen, R.; Moodera, J. S. Temperature dependence of magnetoresistance and surface magnetization in ferromagnetic tunnel junctions. *Physical Review B* **1998**, *58*, R2917-R2920.
- (43) Ye, Y.; Xiao, J.; Wang, H.; Ye, Z.; Zhu, H.; Zhao, M.; Wang, Y.; Zhao, J.; Yin, X.; Zhang, X. Electrical generation and control of the valley carriers in a monolayer transition metal dichalcogenide. *Nature Nanotechnology* **2016**, *11*, 598-602.
- (44) Ochoa, H.; Roldán, R. Spin-orbit-mediated spin relaxation in monolayer MoS₂. *Physical Review B* **2013**, *87*, 245421.
- (45) Wang, L.; Wu, M. W. Electron spin relaxation due to D'yakonov-Perel' and Elliot-Yafet mechanisms in monolayer MoS₂: Role of intravalley and intervalley processes. *Physical Review B* **2014**, *89*, 115302.
- (46) Drögeler, M.; Franzen, C.; Volmer, F.; Pohlmann, T.; Banszerus, L.; Wolter, M.; Watanabe, K.; Taniguchi, T.; Stampfer, C.; Beschoten, B. Spin Lifetimes Exceeding 12 ns in Graphene Nonlocal Spin Valve Devices. *Nano Letters* **2016**, *16*, 3533-3539.
- (47) Park, J.-H.; Lee, H.-J. Out-of-plane magnetoresistance in ferromagnet/graphene/ferromagnet spin-valve junctions. *Physical Review B* **2014**, *89*, 165417.
- (48) Iqbal, M. Z.; Iqbal, M. W.; Lee, J. H.; Kim, Y. S.; Chun, S.-H.; Eom, J. Spin valve effect of NiFe/graphene/NiFe junctions. *Nano Research* **2013**, *6*, 373-380.

- (49) Meng, J.; Chen, J.-J.; Yan, Y.; Yu, D.-P.; Liao, Z.-M. Vertical graphene spin valve with Ohmic contacts. *Nanoscale* **2013**, *5*, 8894-8898.
- (50) Asshoff, P. U.; Sambricio, J. L.; Rooney, A. P.; Slizovskiy, S.; Mishchenko, A.; Rakowski, A. M.; Hill, E. W.; Geim, A. K.; Haigh, S. J.; Fal'ko, V. I.; et al. Magnetoresistance of vertical Co-graphene-NiFe junctions controlled by charge transfer and proximity-induced spin splitting in graphene. *2D Materials* **2017**, *4*, 031004.
- (51) Cobas, E.; Friedman, A. L.; van't Erve, O. M. J.; Robinson, J. T.; Jonker, B. T. Graphene As a Tunnel Barrier: Graphene-Based Magnetic Tunnel Junctions. *Nano Letters* **2012**, *12*, 3000-3004.
- (52) van 't Erve, O. M. J.; Friedman, A. L.; Cobas, E.; Li, C. H.; Robinson, J. T.; Jonker, B. T. Low-resistance spin injection into silicon using graphene tunnel barriers. *Nature Nanotechnology* **2012**, *7*, 737-742.
- (53) Yazyev, O. V.; Pasquarello, A. Magnetoresistive junctions based on epitaxial graphene and hexagonal boron nitride. *Physical Review B* **2009**, *80*, 035408.
- (54) Sanvito, S. Molecular spintronics. *Chemical Society Reviews* **2011**, *40*, 3336-3355.
- (55) Guo, L.; Hu, S.; Gu, X.; Zhang, R.; Wang, K.; Yan, W.; Sun, X. Emerging Spintronic Materials and Functionalities. *Advanced Materials* **2023**, *n/a*, 2301854.
- (56) Piquemal-Banci, M.; Galceran, R.; Godel, F.; Caneva, S.; Martin, M.-B.; Weatherup, R. S.; Kidambi, P. R.; Bouzehouane, K.; Xavier, S.; Anane, A.; et al. Insulator-to-Metallic Spin-Filtering in 2D-Magnetic Tunnel Junctions Based on Hexagonal Boron Nitride. *ACS Nano* **2018**, *12*, 4712-4718.
- (57) Tsymbal, E. Y.; Sokolov, A.; Sabirianov, I. F.; Doudin, B. Resonant Inversion of Tunneling Magnetoresistance. *Physical Review Letters* **2003**, *90*, 186602.
- (58) Kateko, K.; Urbain, E.; Taudul, B.; Schleicher, F.; Arabski, J.; Beaurepaire, E.; Vileno, B.; Spor, D.; Weber, W.; Lacour, D.; et al. Spin-driven electrical power generation at room temperature. *Communications Physics* **2019**, *2*, 116.
- (59) Chowrira, B.; Kandpal, L.; Lamblin, M.; Ngassam, F.; Kouakou, C.-A.; Zafar, T.; Mertz, D.; Vileno, B.; Kieber, C.; Versini, G.; et al. Quantum Advantage in a Molecular Spintronic Engine that Harvests Thermal Fluctuation Energy. *Advanced Materials* **2022**, *34*, 2206688.
- (60) Józsa, C.; Popinciuc, M.; Tombros, N.; Jonkman, H. T.; van Wees, B. J. Controlling the efficiency of spin injection into graphene by carrier drift. *Physical Review B* **2009**, *79*, 081402.
- (61) Zhu, T.; Singh, S.; Katoch, J.; Wen, H.; Belashchenko, K.; Žutić, I.; Kawakami, R. K. Probing tunneling spin injection into graphene via bias dependence. *Physical Review B* **2018**, *98*, 054412.
- (62) Wang, M.; Fu, S.; Petkov, P.; Fu, Y.; Zhang, Z.; Liu, Y.; Ma, J.; Chen, G.; Gali, S. M.; Gao, L.; et al. Exceptionally high charge mobility in phthalocyanine-based poly(benzimidazobenzophenanthroline)-ladder-type two-dimensional conjugated polymers. *Nature Materials* **2023**, *22*, 880-887.
- (63) Dong, J.; Liu, L.; Tan, C.; Xu, Q.; Zhang, J.; Qiao, Z.; Chu, D.; Liu, Y.; Zhang, Q.; Jiang, J.; et al. Free-standing homochiral 2D monolayers by exfoliation of molecular crystals. *Nature* **2022**, *602*, 606-611.
- (64) Zhong, Y.; Cheng, B.; Park, C.; Ray, A.; Brown, S.; Mujid, F.; Lee, J.-U.; Zhou, H.; Suh, J.; Lee, K.-H.; et al. Wafer-scale synthesis of monolayer two-dimensional porphyrin polymers for hybrid superlattices. *Science* **2019**, *366*, 1379-1384.

- (65) Dankert, A.; Pashaei, P.; Kamalakar, M. V.; Gaur, A. P. S.; Sahoo, S.; Rungger, I.; Narayan, A.; Dolui, K.; Hoque, M. A.; Patel, R. S.; et al. Spin-Polarized Tunneling through Chemical Vapor Deposited Multilayer Molybdenum Disulfide. *ACS Nano* **2017**, *11*, 6389-6395.
- (66) Li, W.; Zhou, J.; Cai, S.; Yu, Z.; Zhang, J.; Fang, N.; Li, T.; Wu, Y.; Chen, T.; Xie, X.; et al. Uniform and ultrathin high- κ gate dielectrics for two-dimensional electronic devices. *Nature Electronics* **2019**, *2*, 563-571.
- (67) Zhao, B.; Gan, Z.; Johnson, M.; Najafidehaghani, E.; Rejek, T.; George, A.; Fink, R. H.; Turchanin, A.; Halik, M. 2D van der Waals Heterojunction of Organic and Inorganic Monolayers for High Responsivity Phototransistors. *Advanced Functional Materials* **2021**, *31*, 2105444.